NANO LETTERS

Letter

pubs.acs.org/NanoLett

Yttrium Hydride Nanoantennas for Active Plasmonics

Nikolai Strohfeldt,*[,†] Andreas Tittl,[†] Martin Schäferling,[†] Frank Neubrech,[†] Uwe Kreibig,[‡] Ronald Griessen,[§] and Harald Giessen[†]

[†]4th Physics Institute and Research Center SCoPE, University of Stuttgart, Pfaffenwaldring 57, 70569 Stuttgart, Germany

[‡]1st Physics Institute, RWTH Aachen, Sommerfeldstrasse 14, 52074 Aachen, Germany

[§]Faculty of Sciences, Division of Physics and Astronomy, VU University, De Boelelaan 1081, 1081 HV Amsterdam, The Netherlands

Supporting Information

ABSTRACT: A key challenge for the development of active plasmonic nanodevices is the lack of materials with fully controllable plasmonic properties. In this work, we demonstrate that a plasmonic resonance in top-down nanofabricated yttrium antennas can be completely and reversibly turned on and off using hydrogen exposure. We fabricate arrays of yttrium nanorods and optically observe, in extinction spectra, the hydrogen-induced phase transition between the metallic yttrium dihydride and the insulating trihydride. Whereas the yttrium dihydride nanostructures exhibit a pronounced particle plasmon resonance, the transition to yttrium trihydride leads to a complete vanishing of the resonant behavior. The plasmonic resonance in the dihydride state can be tuned over a wide wavelength range by simply varying the size of the nanostructures. Furthermore, we develop an analytical diffusion model to explain the temporal behavior of the hydrogen loading and unloading trajectories observed in our experiments and gain information about the thermodynamics of our device. Thus, our nanorod system serves as a versatile basic building block for active plasmonic devices ranging from switchable perfect absorbers to active local heating control elements.

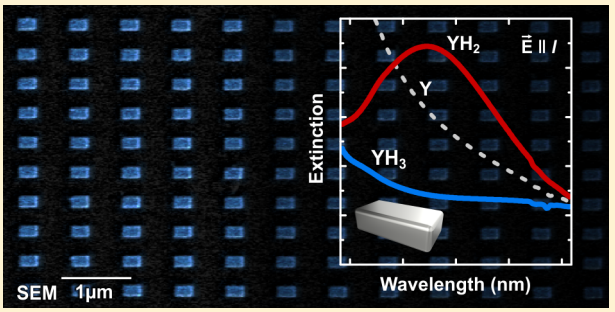

KEYWORDS: *Particle plasmons, active plasmonics, reconfigurable nanostructures, metal−insulator transitions, metal hydrides, switchable mirrors*

Plasmonics has evolved into a broad and important field of nanooptics that enables a variety of new applications.[1−3] By creating local hotspots of the electric field on the nanometer scale, it is possible to develop very sensitive chemical and biological sensor devices and locally initiate and control chemical processes.[4,5] In recent years, plasmonics has expanded toward active nanophotonic devices, which can be reconfigured using external stimuli such as laser pulses,[6] mechanical strain,[7−10] heat,[11] or electrical currents.[12,13] Furthermore, the realization of active plasmonic devices requires a move from widely used but passive metals such as silver or gold toward novel materials systems.[14] This allows for additional degrees of freedom in device design and enables external control over the optical response of a plasmonic nanostructure without having to directly modify its geometry.[15,16]

Phase change materials provide an ideal toolkit for the realization of such active nanodevices and several materials with heating- or laser-induced switching behavior such as vanadium dioxide (VO_2),[11,17−19] gallium lanthanum sulphide (GLS),[20] or germanium antimony telluride (GST)[21−23] have already been investigated in the context of plasmonics.

In 1996, Huiberts et al.[24] discovered a switchable mirror effect in thin films of yttrium when exposed to hydrogen gas. They demonstrated that a fully reflecting metallic yttrium mirror becomes dielectric and almost completely transparent after absorbing a sufficient amount of hydrogen. This work was expanded to the field of nanoparticles by Stepanov et al.,[25,26] who showed that hydrogenated spherical yttrium nanoparticles under ultrahigh vacuum conditions can have switchable Mie resonances.

Here, we demonstrate reconfigurable YH_x nanoantennas, fabricated via electron beam lithography, which exhibit a pronounced plasmonic resonance in their metallic YH_2 state. The resonance wavelength and width can be widely tuned through variation of the antenna dimensions. Compared to the very small, bottom-up produced nanoparticles from Stepanov et al.,[25,26] we demonstrate antennas and antenna assemblies with a large oscillator strength and varying size, showing custom-designed plasmonic properties in the near- and mid-IR spectral regions. The transition between metallic and dielectric yttrium hydride antennas is induced by simple hydrogen exposure from the gas phase or from electrolysis under ambient atmospheric conditions and shows a drastic change of the spectral response.

Compared to other promising phase change materials used in plasmonic devices, yttrium dihydride has the advantage of comparatively low intrinsic damping and can therefore support

Received: September 30, 2013
Revised: January 26, 2014
Published: February 27, 2014

plasmonic resonances itself, whereas the metallic phases of VO_2, GST, or GLS are known to exhibit only a weak plasmonic response, if any. Despite the advantage of much faster switching times, they can often be used only in hybrid plasmonic systems, that is, in combination with gold or other good plasmonic metals. However, the use of hybrid systems drastically lowers the switching contrast, since only the dielectric environment of the resonant material changes and not the antenna itself. Therefore, yttrium dihydride is a highly relevant and very promising alternative for plasmonic applications that require a high switching contrast and are less dependent on ultrashort switching times. Furthermore, as a metal, yttrium and its hydrides can be structured easily using standard nanofabrication techniques.

During hydrogen absorption, metallic yttrium (Y) transforms first into yttrium dihydride (YH_2, Figure 1a), which has an even

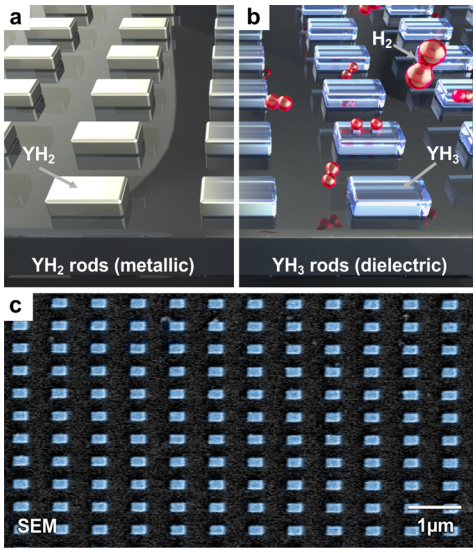

Figure 1. (a) Schematic drawing of a metallic yttrium dihydride (YH_2) nanorod array on a fused silica substrate in hydrogen-free environment. (b) Formation of dielectric yttrium trihydride (YH_3) nanorods under hydrogen exposure. (c) Exemplary SEM image of the fabricated YH_2 nanorods.

higher electrical conductivity than pure yttrium. This phase change from a metal in hcp configuration into a fcc metal is nonreversible under normal conditions. Through further exposure to hydrogen, it undergoes a second, reversible, phase change into yttrium trihydride (YH_3, Figure 1b), a transparent semiconductor with a hcp structure. However, it is important to note that under normal hydrogen partial pressures (i.e., less than 1 bar near room temperature) full stoichiometric YH_3 cannot be realized,[27] and the final state of the system reaches only $YH_{3-\delta}$, where δ is in the range of 0.1−0.3 (under very high pressure δ = 0.01 can be reached[28]). For simplicity, we will refer to this final state as yttrium trihydride (YH_3).

The transition from YH_2 to YH_3 induces strong and reversible changes in the dielectric properties that can be triggered at low partial pressures of hydrogen. Even though yttrium hydride thin films exhibit a large hysteresis effect,[29] the ability to switch reversibly (in the sense that after a full hysteresis loop it returns to the original dihydride phase) from metal to a transparent semiconductor upon hydrogen absorption makes yttrium an attractive candidate for active plasmonic applications. Moreover, due to the drastic change from metal to insulator, the plasmonic response vanishes completely when the yttrium is in the trihydride phase and recovers when switched back into the yttrium dihydride phase.

To demonstrate the functionality of such a switchable plasmonic system, we fabricate arrays of yttrium nanorods (Figure 1c). We choose nanorods as a model system because they exhibit a strong plasmonic response and approximately dipole-like behavior and therefore constitute an ideal development platform for new plasmonic materials such as yttrium dihydride.

To realize this system experimentally, we first prepare a PMMA mask on a fused silica substrate using a standard electron beam lithography process.[30] Afterward, yttrium and platinum are evaporated onto the developed PMMA mask via electron beam assisted evaporation. Platinum on top of the yttrium rods serves as a catalytic layer to dissociate the H_2 molecules into atomic hydrogen. Hydrogen can then be incorporated into the yttrium lattice to form the hydride states. Catalytic materials such as platinum or palladium next to yttrium are necessary because yttrium itself is not able to catalytically dissociate H_2 molecules into atomic hydrogen. Additionally, the platinum cover prevents oxidation at the top surface of the yttrium rods. Such oxidation is common in transition metals like yttrium, which easily form an oxide layer (Y_2O_3) of several nanometers when exposed to oxygen.[26] This impedes hydrogen from penetrating into the particle volume. Although the thin layer of platinum introduces some additional damping to our system, the overall influence on the plasmonic response is weak.

Figure 2 shows typical extinction spectra of the different hydrogenation states of yttrium nanoantennas measured with a

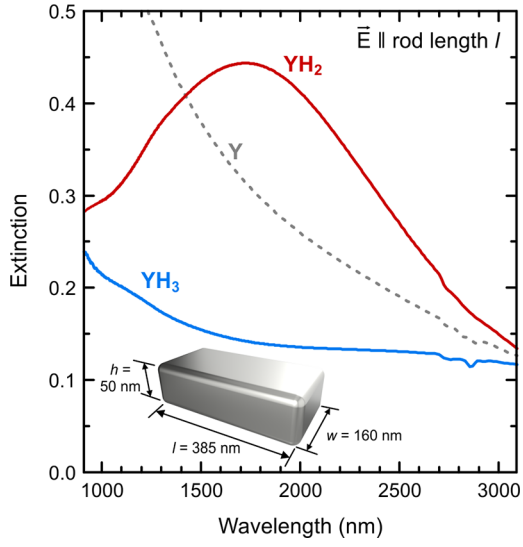

Figure 2. Extinction spectra of yttrium, YH_2, and YH_3 nanorods. The metallic YH_2 rods (red line) show a distinct particle plasmon resonance at 1720 nm. In contrast, the YH_3 rods (blue line) are almost transparent in the same spectral region. The increased extinction in Y nanorods (gray dotted line) toward lower wavelengths can be attributed to the tail of a broad electronic transition in yttrium occurring at around 400 nm which makes them unsuitable for plasmonic applications.

commercial Fourier transform infrared spectroscopy system (Bruker FTIR) and an incident electric field polarization parallel to the rods. Here, the rods have dimensions of 385 × 160 nm and a height of 50 nm yttrium plus 6 nm platinum.

Pure yttrium is a metal with a relatively low electrical conductivity,[31,32] and therefore Y nanoantennas do not exhibit

dx.doi.org/10.1021/nl403643v | *Nano Lett.* 2014, 14, 1140−1147

a distinct plasmonic response in the visible and near-IR spectral region (gray dotted line in Figure 2). The decrease in extinction toward longer wavelengths can be attributed to the tail of a very strong and broad electronic resonance at about 3.1 eV (400 nm).[33] In contrast to Y, YH_2 is a good metal with a markedly different atomic and electronic structure.[26,34,35] To transform the yttrium into YH_2, we expose our sample to 4 vol % hydrogen in nitrogen for 10 min. According to literature, this is more than sufficient to reach the dihydride and even the trihydride state.[36] However, the transition between Y and YH_2 is nonreversible at room temperature, whereas the second transition between YH_2 and YH_3 is fully reversible. Therefore the rods automatically settle in the YH_2 state after the hydrogen is turned off and equilibrium is reached.

The red line in Figure 2 shows an extinction spectrum of such a hydrogenated rod array in the YH_2 state. The YH_2 rods have a clear extinction maximum at approximately 1720 nm that can be attributed to a localized surface plasmon resonance. This YH_2 state can be seen as the ground state of our switchable plasmonic structure, because the system will not return to the unhydrided state without extremely harsh and destructive measures such as strong heating and ultrahigh vacuum. Therefore the yttrium nanostructure can only be switched reversibly between the dihydride and the trihydride phase. This is not a disadvantage as there is a large contrast in extinction between YH_2 and YH_3 (see Figure 2).

When continuously exposed to hydrogen (in this case 5 vol % H_2 in N_2 at room temperature), the yttrium nanostructures switch into the trihydride phase within seconds. This dramatic change from a metal to a Mott insulator also leads to a drastic change in the extinction spectrum. In fact, yttrium hydride is one of the few strongly correlated systems with a continuous Mott–Hubbard metal–insulator transition.[37,38]

The particle plasmon resonance fully vanishes, and the extinction spectrum becomes almost flat, as shown by the blue line in Figure 2. This proves that it is possible to completely turn off the plasmon resonance by introducing only small and safe amounts of hydrogen into the system. The switching results in a relative extinction change at the peak wavelength (1720 nm) of almost 70%, which translates to an absolute change in transmittance of 23% that can easily be observed by the naked eye.

To incorporate yttrium nanostructures into switchable plasmonic devices, the ability to tune the plasmon resonance over a wide spectral range is needed. Here, the simplest approach is to vary the length of the plasmonic nanorods while leaving width and height constant.

Consequently, we fabricated yttrium rod arrays with a constant width w of 160 nm and height h of 50 nm yttrium covered with 6 nm platinum, while varying the length from 290 to 385 nm. Figure 3 shows the change of the plasmon resonance for increasing rod length. For longer rods, we observe a higher extinction as well as a red-shift of the resonance wavelength. The increasing extinction can be attributed to the enhanced dipole strength that is caused by the increase in nanoparticle volume. A further contribution comes from the increased filling factor of the arrays, since we keep the periodicity (p_x = 700 nm; p_y = 400 nm) unchanged for all rod lengths. The red-shift of about 400 nm is a clear indication of a particle plasmon resonance that is highly correlated with particle dimension and shape. Especially, we find a linear relation between rod length l and plasmon resonance wavelength λ_{res}, shown in the inset of Figure 3, which is in excellent agreement with theoretical and experimental knowledge about plasmon resonances in metal nanoantennas.[39,40] The tuning range of our reconfigurable antennas is mainly limited at lower wavelengths due to a broad electronic transition at around 400 nm. At longer wavelengths, the YH_2 dielectric function follows a Drude-like behavior and thus enables full tunability of the plasmonic resonance.

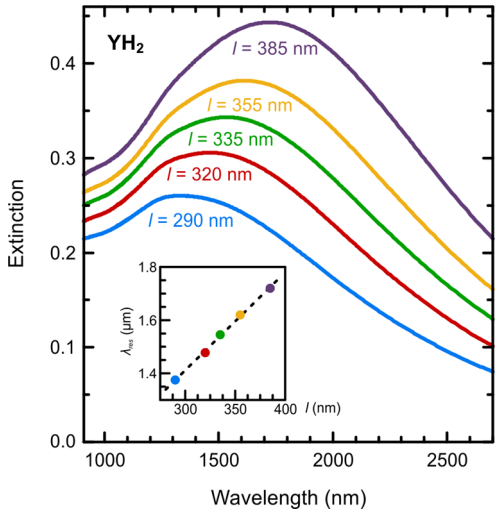

Figure 3. YH_2 extinction spectra for various rod lengths l and constant width (w = 160 nm) and height (h = 50 nm), showing a red-shift and increase in amplitude of the resonance for increasing rod lengths. The inset shows the extracted particle plasmon peak positions (colored dots) that scale linearly with rod length ($\lambda_{res} = 4.2l + 115$ nm), as indicated by the black dashed line.

To investigate the switching dynamics in our nanoantenna system in more detail, we study the temporal behavior of the extinction during hydrogen exposure. Figure 4 shows the H_2 loading (Figure 4a, b) and the unloading process (Figure 4c, d) of an yttrium rod array with rod parameters l = 290 nm, w = 160 nm, h_Y = 50 nm, h_{Pt} = 6 nm, and a periodicity $p_{x,y}$ = 400 nm, measured at room temperature. We start in the YH_2 phase and observe a strong resonance at 1580 nm (red line, Figure 4a). After exposing the system to hydrogen (5 vol % H_2 in N_2), the resonance immediately flattens and continuously approaches the YH_3 spectrum where it saturates after approximately 50 s (blue line). The spectra in Figure 4a show a typical set of FTIR measurements recorded during hydrogen uptake with one measurement every 4 s. In Figure 4b the extinction time trace at 1580 nm (position of the YH_2 plasmon resonance) is displayed (green line), showing the almost instantaneous reaction to hydrogen exposure. Within a few seconds, the extinction starts to drop from 0.62 with an almost constant slope of 2% per second. This large change together with the reasonable response time makes the system well-suited for active plasmonic devices. Moreover, the switching time from the dihydride to the trihydride phase decreases monotonically with the hydrogen pressure as shown in the Supporting Information and explained by the diffusion model below.

Figure 4c shows the back reaction, moving from YH_3 to YH_2. This takes approximately 3 h, which is significantly slower than the absorption reaction. There are several factors that lead to this slow transition. The key reason is the reduced out-diffusion of hydrogen due to the platinum cap layer and the oxidized sidewalls of the nanoantennas.

To explain this asymmetry in the behavior of our system, we developed an analytical one-dimensional diffusion model,

dx.doi.org/10.1021/nl403643v | Nano Lett. 2014, 14, 1140–1147

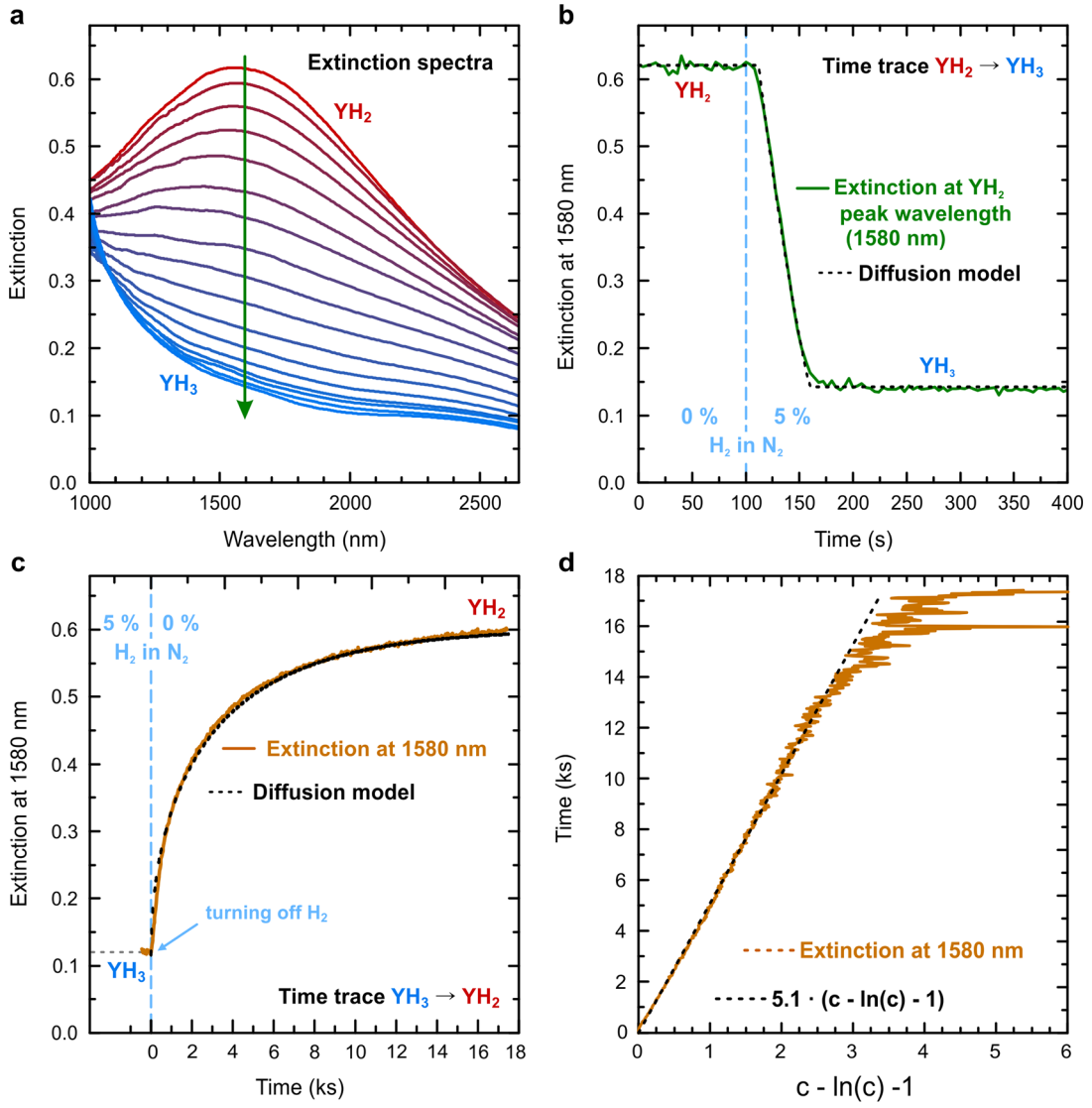

Figure 4. In situ hydrogenation dynamics of the yttrium nanorods at room temperature. (a) Extinction spectra taken every 4 s during hydrogen exposure. The phase transition from the metallic YH_2 (red lines) to the dielectric YH_3 (blue lines) can be clearly observed. (b) Full time trace of the measured extinction at a wavelength of 1580 nm. After 100 s the sample is exposed to 5 vol % hydrogen in nitrogen at constant pressure of 1 bar. The system almost instantly reacts and switches to the dielectric YH_3 state. The phase transition is completed within less than 50 s. The black dashed line shows the fit to our diffusion model. (c) When turning off the hydrogen exposure the system relaxes back into the metallic YH_2 state (orange line). (d) Time trace of (c) renormalized to a range between 0 and 1 (named c for concentration) and then plotted as time versus $c - \ln c - 1$ (orange line). The resulting straight line demonstrates the validity of our analytical diffusion model. The slope (5100 s) of the best fit straight line (black dashed line) yields the fitting parameter τ/f (see eq 7).

following the ideas of Pasturel et al.[41] The assumption of a 1D system is valid, since the oxidized side walls of the nanorods channel the hydrogen flow through the platinum cap layer in and out of the yttrium-hydride nanostructures. The model incorporates the diffusion of atomic hydrogen through the caplayer and into the Y nanoantenna. Soon after exposition to hydrogen gas at pressure p_{H2}, a stationary state is established with a linear concentration gradient in the caplayer. The H current through the caplayer is then equal to the diffusion current into the Y antennas, and we have

$$j_{\text{diffusion}} = \frac{D_{\text{Pt}}}{V_{\text{Pt}}}\frac{c_s - c_i}{L_{\text{Pt}}} = \frac{L_Y}{V_Y}\frac{dc_Y}{dt} \tag{1}$$

where L_{Pt} is the thickness of the Pt cap layer, D_{Pt} the diffusion coefficient of H in Pt, L_Y the thickness of Y, and V_{Pt} and V_Y the molar volumes of Pt and Y, respectively. The H concentrations in the Pt layer are c_s at the surface and c_i at the Pt−Y interface. The H concentration in Y is c_Y. Using the fact that the chemical potential of H in the sample is continuous everywhere, we derive the following relations between c_s, c_i, c_Y, and the hydrogen loading pressure p_{H2}.

$$c_s = g\sqrt{p_{H2}} \quad \text{and} \quad c_i = f\frac{c_Y}{1 - c_Y} \tag{2}$$

with

$$g = \exp\left(-\frac{\Delta H_{\text{Pt}} + (1/2)TS_{H2}}{RT}\right) \quad \text{and}$$

$$f = \exp\left(\frac{\Delta H_Y - \Delta H_{\text{Pt}}}{RT}\right) \tag{3}$$

dx.doi.org/10.1021/nl403643v | Nano Lett. 2014, 14, 1140−1147

where ΔH_{Pt} and ΔH_Y are the enthalpy of hydrogen absorption in Pt and Y, respectively, and S_{H2} is the entropy of gaseous H_2 at 1 bar.

Combining eqs 1 and 2, we obtain a differential equation for the hydrogen concentration c_Y:

$$\frac{dc_Y}{dt} = \frac{m}{\tau}\left(g\sqrt{p} - f\frac{c_Y}{1-c_Y}\right) \quad (4)$$

where $\tau = L_{Pt}L_Y/D_{Pt}$ and $m = V_Y/V_{Pt} = 19.88/9.09 = 2.19$ is the ratio between the molar volumes of Y and Pt. In the case of hydrogen loading eq 4 can be solved and approximated by a straight line for sufficiently low concentrations c_Y, leading to

$$c_Y(t) \cong \frac{mg}{\tau}\sqrt{p_{H2}} \times t \quad (5)$$

The measured loading curve in Figure 4c resembles this linear behavior very well and by normalizing the measured extinction values to the interval [0,1], one finds $mg(p_{H2})^{1/2}/\tau = 1/46$ and, since $p_{H2} = 0.05$ bar during loading, $mg/\tau = 0.097$/bar.

During unloading of the antennas in vacuum, that is, at $p_{H2} = 0$, we have

$$\frac{dc_Y}{dt} = -\frac{mf}{\tau}\left(\frac{c_Y}{1-c_Y}\right) \quad (6)$$

which is readily integrated to

$$t = \frac{\tau}{mf}\left(c_Y - c_\infty + \ln\left(\frac{c_\infty}{c_Y}\right)\right) \quad (7)$$

Under the chosen experimental conditions we expect c_∞ to be close to unity. A plot of time versus $c_Y - 1 - \ln c_Y$ should thus be a straight line with slope $\tau/(mf)$. This is indeed the case. Figure 4d shows the measured unloading data from Figure 4c normalized to the range from 1 to 0 (orange line) plotted in this way. The measured data points follow a straight line with slope $\tau/(mf) = 5100$ s. Deviations at higher times (for c close to 0) are merely due to noise in the measurement data. The excellent agreement between model and experimental data for both hydrogen loading and unloading strongly supports the validity of the assumptions made in its derivation. For $m = 2.19$, we find $f/\tau = 9 \times 10^{-5}$ s^{-1}.

With $D_{Pt} = 3 \times 10^{-7}$ cm^2/s derived from an extrapolation of Katsuta and McLellan diffusity data[42] to room temperature, we find $\tau = L_{Pt}L_Y/D_{Pt} = 1 \times 10^{-5}$ s and thus $f = 9 \times 10^{-10}$. From the definition of f and $\Delta H_Y \cong -40$ kJ/mol H from Van Gogh et al.[31] we find $\Delta H_{Pt} \cong +8$ kJ/mol H for the enthalpy of hydrogen solution for the platinum layer. This value is smaller than $\Delta H_{Pt} \cong +35$ kJ/mol H for bulk Pt.[43] This might be due to partial alloying of Pt with the underlying Y (the enthalpy of, for example, a Y−Pt alloy is very negative,[44] −247 kJ/mol) and to surface roughness of the thin ($L_{Pt} = 6$ nm) caplayer. One should also realize that large lattice expansions occurred during the initial loading of the antenna from pure Y to dihydride YH_2.

By carrying out loading experiments at 0.05, 0.1, and 0.2 bar hydrogen pressure with a different sample we found that $(dc_Y/dt)/(p_{H2}{}^{1/2})$ remains constant (see the Supporting Information), which is in agreement with eq 5.

At this point the reader might wonder whether the large asymmetry between loading and unloading times is due to a particular choice of parameters. It is in fact easy to show that it is a robust property only related to the low solubility of H in the cap layer. From eq 1 follows that the H particle current is proportional to $c_s - c_i$. At half loading, that is, when $c_Y = 0.5$, $c_i = f$ according to eq 2. During unloading the driving gradient is $c_s - c_i = -c_i = -f$ as the surface concentration is at best 0. During loading, however, relatively large values of the surface concentration can be set up so that $c_s - f \gg f$. For metals with a low solubility f is very small (for Pt, $f = 2 \times 10^{-9}$, see above), and $c_s \gg 2f$ is already satisfied at relatively low pressures (in our case, certainly for $p > 0.01$ bar).

In summary, we can say that the asymmetry between the loading and unloading times can be explained by the high (and in this case even positive) solution enthalpy of platinum. Since this enthalpy depends on the nanoscale structure and thickness of the platinum, it will be of interest to conduct further studies on the optimal thickness and material of the capping layer to obtain shorter switching times without interfering with the plasmonic properties of the system. Even without such optimizations, both the diffusion limited absorption and the desorption processes can be accelerated by heating the sample.

Good agreement between experimental results and theoretical/numerical predictions is crucial for the efficient and robust design of switchable devices. To verify this for our yttrium nanoantenna system, we perform numerical simulations of the optical response using a commercial FEM solver (CST Microwave Studio). The optical constants of yttrium and the different hydrides are taken from literature.[31,45] Here, the dielectric functions of $YH_{1.8}$ and $YH_{2.9}$ from ref 25 provide the closest match to the yttrium hydride states that were investigated in our measurements and identified as YH_2 and YH_3, respectively. The numerical results for such $YH_{1.8}$ and $YH_{2.9}$ nanorod arrays are presented in the Supporting Information (Figure S2).

Whereas the $YH_{2.9}$ results are in good agreement with the measured data (almost flat response), the $YH_{1.8}$ spectra require closer attention. Figure 5 shows the numerical results for an $YH_{1.8}$ (50 nm) + Pt (6 nm) nanorod array on a fused silica substrate as a green dotted line. In this simulation we use the complex dielectric function of $YH_{1.8}$ from Van Gogh et al.,[31] and Pt from Weaver,[46] respectively. The rods are assumed to have dimensions of 380 × 160 × 56 nm and periodicities of 700 × 400 nm in accordance with SEM measurements on the fabricated structures. The measured spectrum is shown as a solid black line in Figure 5. Comparing the black solid and green dotted line, we can observe significant differences. The numerical extinction peak is much narrower, higher in amplitude, and red-shifted compared to the measured one.

Since both experiment and simulation return absolute values for the extinction, the reason for the significant quantitative deviation has to be found in the modeling of the simulated nanorod system itself.

One major deviation between the model and the experimental system is the yttrium oxide (Y_2O_3) layer that forms at all yttrium surfaces that are not protected from oxygen. This layer has a thickness of a few nanometers[26,32] and forms at the side walls of the yttrium rods that are not protected by either the substrate or the platinum cover layer. If we assume an oxide thickness of 3 nm and replace the outermost 3 nm in our model's sidewalls with dielectric Y_2O_3 using a constant refractive index[47] of $n = 1.93$, we obtain the dashed green line in Figure 5. Even though the discrepancy between simulation and experiment is slightly reduced, there is still a key ingredient missing to match the experimental data.

In our previous calculations, we have used a dielectric function of YH_2 measured on extended thin films with thicknesses in the 300 nm range, prepared and characterized under ultrahigh

dx.doi.org/10.1021/nl403643v | Nano Lett. 2014, 14, 1140−1147

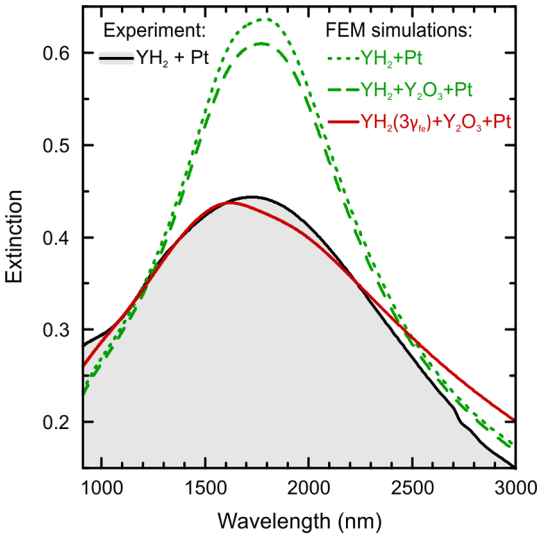

Figure 5. Comparison of the experiment to FEM simulations of the yttrium rod system. The black line shows the experimental spectrum of an YH_2 nanorod array with parameters l = 380 nm;w = 160 nm; h_{YH2} = 50 nm; h_{Pt} = 6 nm. The green lines show simulated data for the same system using tabulated dielectric data. However, the simulated spectra for YH_2 rods with a platinum cover (green dotted line) show a resonance, which is much narrower and slightly red-shifted compared to the experimental data. This mismatch cannot be compensated by simply introducing a surrounding yttrium oxide shell (dashed green line) into the simulation. Only an additional increase of the free electron damping γ_{fe} in the YH_2 dielectric function by a factor of 3 is able the reproduce the experimental data fully (red line).

vacuum conditions.[31] In comparison, our nanostructuring process (PMMA masking, electron-beam assisted evaporation) can introduce impurities and defects into our nanorod system.

Combined with the higher reactivity of yttrium and its desire to form yttrium oxide, this leads to a deterioration of the plasmonic properties. This effect becomes especially pronounced when moving from extended films to nanoparticle structures. One way of measuring the impact of the nanostructuring on the yttrium dielectric function quantitatively would be to perform ellipsometry on such a nanorod array. However, this is not feasible due to the low reflectance of the arrays at glancing angles.

In general, surface modifications as well as impurities in a plasmonic material lead to a decreased free electron lifetime τ_{fe} compared to the film that was used in ref 25 and therefore an enhanced free electron damping $\gamma_{fe} = (1/\tau_{fe})$ in our system.

To modify the dielectric function of yttrium dihydride with this assumption, we first fit a Drude model together with a harmonic oscillator to the YH_2 dielectric data following the approach of Gartz and Quinten for unhydrided yttrium.[48] This model (more detailed discussion in the Supporting Information, Figure S3) yields the free electron damping γ_{fe}, the plasma frequency ω_p, the oscillator strength S_{oz}, and the oscillator frequency and damping ω_{oz}, γ_{oz} as fitting parameters. However, in the near-infrared region (NIR) where our particle plasmon resonance is located, the YH_2 can be seen as an almost perfect Drude metal with a dielectric function $\varepsilon(\omega)$ which is mostly governed by the free electron damping γ_{fe} and the plasma frequency ω_p. Therefore, we can safely ignore the oscillator part of the model in our discussion.

If we now want to incorporate the previously discussed impurities and defects into our simulation, we can increase the free electron damping in the dielectric function without changing the other parameters. Increasing the damping constant by a factor of 3 from $\gamma_{fe} = 2.4 \times 10^{14}$ s^{-1} to $\gamma^*_{fe} = 7.2 \times 10^{14}$ s^{-1} is reasonable, since the nanofabrication process strongly alters the structure of the yttrium compared to yttrium films used for ellipsometry measurements in literature.

With all influences included (platinum cover, yttrium oxide layer, enhanced intrinsic damping), we obtain excellent agreement with the measured data, as exemplified by the red line in Figure 5, verifying the hypothesis of an increased intrinsic damping in our samples.

In conclusion, we have shown that yttrium nanostructures offer an exciting new pathway for the design of active plasmonic devices by utilizing hydrogen-induced metal insulator transitions. We have demonstrated that YH_2 nanorods exhibit a pronounced particle plasmon resonance in the NIR which can be tuned over a wide spectral range. This resonance can be switched off within several seconds by introducing hydrogen into the system that transforms the nanorods into dielectric YH_3. After the hydrogen exposure is stopped, the plasmonic resonance slowly returns to its original form, demonstrating the full reversibility of the transition. In addition, we found a way to model this diffusion process analytically and gain knowledge about the thermodynamic quantities of our system. This gives us the ability to further improve the material system in the future on the road to a fast and reliable switching device. Therefore we also modeled the dielectric properties and the plasmonic behavior of our YH_2 nanoantennas. These results provide a powerful tool to predict the behavior of any yttrium based plasmonic nanodevice and even allow us to make quantitative predictions about the resonance width and position of more complex structures.

In the future, yttrium nanostructures can form a crucial building block in the realization of a variety of plasmonic switching schemes. Possible applications include switchable plasmonic EIT[49] or switchable perfect absorber devices[50] where the hydrogen concentration can be adjusted by adjusting the voltage in a simple electrochemical cell setup.[51] Furthermore, the system can be used as a hydrogen detector through monitoring the slope of YH_2 to YH_3 phase transition or to locally control chemical processes that require a certain activation energy. This energy can be provided by the enhanced local electric field generated by the plasmonic resonance, depending on the surrounding hydrogen concentration. Due to its high refractive index, YH_3 could even act as high-index nanophotonic material ($n \approx 2.8$ at 600 nm[31,52]) which supports electric and magnetic Mie resonances[53,54] that can be switched on and off using hydrogen. Other transition metals such as vanadium[55] or scandium, or transition metal alloys like Mg–Y, Mg–La, Mg–Sc, and Mg–Gd may provide even faster response.[56−59] Complete blackness and thus highest switching contrast could be expected using nickel metal hydrides (such as Mg_2MeH_x, with Me = Ni, Co, Fe).[60] Finally, studies of the Mott–Hubbard metal-to-insulator phase transition in rare earth and lanthanide hydride nanostructures as a function of structure size, morphology, and so forth, will enable a whole family of intriguing experiments.

■ ASSOCIATED CONTENT

Supporting Information

Optical characterization, details of the diffusion model, and description of the extinction simulations and the dielectric function modeling. This material is available free of charge via the Internet at http://pubs.acs.org.

dx.doi.org/10.1021/nl403643v | Nano Lett. 2014, 14, 1140−1147

AUTHOR INFORMATION

Corresponding Author

*E-mail: n.strohfeldt@pi4.uni-stuttgart.de.

Notes

The authors declare no competing financial interest.

ACKNOWLEDGMENTS

We gratefully acknowledge financial support by the Deutsche Forschungsgemeinschaft (SPP1391, FOR730, and GI 269/11-1), by the Bundesministerium für Bildung und Forschung (13N9048 and 13N10146), by ERC Advanced Grant COMPLEXPLAS, by the Baden-Württemberg Stiftung (Spitzenforschung II) and by the Ministerium für Wissenschaft, Forschung und Kunst Baden-Württemberg (Az: 7533-7-11.6-8). We would like to thank Heinz Schweizer for very interesting and fruitful discussions.

REFERENCES

(1) Maier, S. A. *Plasmonics: Fundamentals and Applications*, 1st ed.; Springer: New York, 2007; p 223.
(2) Halas, N. J.; Lal, S.; Chang, W.-S.; Link, S.; Nordlander, P. *Chem. Rev.* **2011**, *111*, 3913−61.
(3) Giannini, V.; Fernández-Domínguez, A. I.; Heck, S. C.; Maier, S. A. *Chem. Rev.* **2011**, *111*, 3888−912.
(4) Christopher, P.; Xin, H.; Marimuthu, A.; Linic, S. *Nat. Mater.* **2012**, *11*, 1−7.
(5) Lal, S.; Link, S.; Halas, N. J. *Nat. Photonics* **2007**, *1*, 641−648.
(6) Traviss, D.; Bruck, R.; Mills, B.; Abb, M.; Muskens, O. L. *Appl. Phys. Lett.* **2013**, *102*, 121112.
(7) Zhu, X.; Shi, L.; Liu, X.; Zi, J.; Wang, Z. *Nano Res.* **2010**, *3*, 807−812.
(8) Pryce, I. M.; Aydin, K.; Kelaita, Y. A.; Briggs, R. M.; Atwater, H. A. *Nano Lett.* **2010**, *10*, 4222−7.
(9) Qian, X.; Park, H. S. *J. Mech. Phys. Solids* **2010**, *58*, 330−345.
(10) Olcum, S.; Kocabas, A.; Ertas, G.; Atalar, A.; Aydinli, A. *Opt. Express* **2009**, *17*, 8542−7.
(11) Appavoo, K.; Lei, D. Y.; Sonnefraud, Y.; Wang, B.; Pantelides, S. T.; Maier, S. A.; Haglund, R. F. *Nano Lett.* **2012**, *12*, 780−6.
(12) Emani, N. K.; Chung, T.-F.; Ni, X.; Kildishev, A. V.; Chen, Y. P.; Boltasseva, A. *Nano Lett.* **2012**, *12*, 5202−6.
(13) Ou, J.-Y.; Plum, E.; Zhang, J.; Zheludev, N. I. *Nat. Nanotechnol.* **2013**, *8*, 252−5.
(14) Naik, G. V.; Shalaev, V. M.; Boltasseva, A. *Adv. Mater.* **2013**, *25*, 3264−94.
(15) Vivekchand, S. R. C.; Engel, C. J.; Lubin, S. M.; Blaber, M. G.; Zhou, W.; Suh, J. Y.; Schatz, G. C.; Odom, T. W. *Nano Lett.* **2012**, *12*, 4324−4328.
(16) Soares, B.; Jonsson, F.; Zheludev, N. *Phys. Rev. Lett.* **2007**, *98*, 153905.
(17) Driscoll, T.; Palit, S.; Qazilbash, M. M.; Brehm, M.; Keilmann, F.; Chae, B.-G.; Yun, S.-J.; Kim, H.-T.; Cho, S. Y.; Jokerst, N. M.; Smith, D. R.; Basov, D. N. *Appl. Phys. Lett.* **2008**, *93*, 024101.
(18) Dicken, M. J.; Aydin, K.; Pryce, I. M.; Sweatlock, L. A.; Boyd, E. M.; Walavalkar, S.; Ma, J.; Atwater, H. A. *Opt. Express* **2009**, *17*, 18330−9.
(19) Lei, D. Y.; Appavoo, K.; Sonnefraud, Y.; Haglund, R. F.; Maier, S. A. *Opt. Lett.* **2010**, *35*, 3988−90.
(20) Sámson, Z. L.; MacDonald, K. F.; De Angelis, F.; Gholipour, B.; Knight, K.; Huang, C. C.; Di Fabrizio, E.; Hewak, D. W.; Zheludev, N. I. *Appl. Phys. Lett.* **2010**, *96*, 143105.
(21) Chen, Y.; Kao, T.; Ng, B.; Li, X. *Opt. Express* **2013**, *21*, 1566−1569.
(22) Gholipour, B.; Zhang, J.; MacDonald, K. F.; Hewak, D. W.; Zheludev, N. I. *Adv. Mater.* **2013**, *25*, 3050−4.
(23) Michel, A.-K. U.; Chigrin, D. N.; Maß, T. W. W.; Schönauer, K.; Salinga, M.; Wuttig, M.; Taubner, T. *Nano Lett.* **2013**, *13*, 3470−3475.
(24) Huiberts, J. N.; Griessen, R.; Rector, J. H.; Wijngaarden, R. J.; Dekker, J. P.; de Groot, D. G.; Koeman, N. J. *Nature* **1996**, *380*, 231−234.
(25) Stepanov, A. L.; Bour, G.; Reinholdt, A.; Kreibig, U. *Tech. Phys. Lett.* **2002**, *28*, 642−644.
(26) Stepanov, A. L.; Bour, G.; Gartz, M.; Osin, Y. N.; Reinholdt, A.; Kreibig, U. *Vacuum* **2001**, *64*, 9−14.
(27) Kooij, E. S.; van Gogh, A. T. M.; Nagengast, D. G.; Koeman, N. J.; Griessen, R. *Phys. Rev. B* **2000**, *62*, 10088−10100.
(28) Huiberts, J.; Griessen, R.; Wijngaarden, R.; Kremers, M.; Van Haesendonck, C. *Phys. Rev. Lett.* **1997**, *79*, 3724−3727.
(29) Remhof, A.; Kerssemakers, J.; van der Molen, S.; Griessen, R.; Kooij, E. S. *Phys. Rev. B* **2002**, *65*, 054110.
(30) Hentschel, M.; Schäferling, M.; Metzger, B.; Giessen, H. *Nano Lett.* **2013**, *13*, 600−6.
(31) Van Gogh, A.; Nagengast, D.; Kooij, E.; Koeman, N.; Rector, J.; Griessen, R.; Flipse, C.; Smeets, R. *Phys. Rev. B* **2001**, *63*, 195105.
(32) Bour, G.; Reinholdt, A.; Stepanov, A.; Keutgen, C.; Kreibig, U. *Eur. Phys. J. D* **2001**, *16*, 219−223.
(33) Gartz, M.; Quinten, M. *Appl. Phys. B: Lasers Opt.* **2001**, *73*, 327−332.
(34) Vajda, P. In *Handbook on the Physics and Chemistry of Rare Earths*, Vol. *20*; Gschneidner, K. A., Eyring, J., Lander, G. H., Eds.; Elsevier: New York, 1995; pp 207−291.
(35) Aruna, I.; Malhotra, L. K.; Mehta, B. R. In *Handbook on the Physics and Chemistry of Rare Earths*; Gschneidner, K. A., Bunzli, J.-C. G., Pecharsky, V. K., Eds.; Elsevier: New York, 2006; Vol. *36*, pp 83−279.
(36) Kooij, E. S.; van Gogh, A. T. M.; Griessen, R. *J. Electrochem. Soc.* **1999**, *146*, 2990.
(37) Hoekstra, A. F. T.; Roy, A. S.; Rosenbaum, T. F. *J. Phys.: Condens. Matter* **2003**, *15*, 1405−1413.
(38) Hoekstra, A.; Roy, A.; Rosenbaum, T.; Griessen, R.; Wijngaarden, R.; Koeman, N. *Phys. Rev. Lett.* **2001**, *86*, 5349−5352.
(39) Bryant, G. W.; García de Abajo, F. J.; Aizpurua, J. *Nano Lett.* **2008**, *8*, 631−6.
(40) Dattoma, T.; Grande, M.; Marani, R.; Morea, G.; Marrocco, V.; D'Orazio, A. *Prog. Electromagn. Res. B* **2011**, *30*, 337−353.
(41) Pasturel, M.; Wijngaarden, R. J.; Lohstroh, W.; Schreuders, H.; Slaman, M.; Dam, B.; Griessen, R. *Chem. Mater.* **2007**, *19*, 624−633.
(42) Katsuta, H.; McLellan, R. B. *J. Phys. Chem. Solids* **1979**, *40*, 697−699.
(43) Griessen, R.; Riesterer, T. In *Hydrogen in Intermetallic Compounds I SE - 6*; Schlapbach, L., Ed.; Springer: Berlin, 1988; Vol. *63*, pp 219−284.
(44) Buschow, K. H. J.; Bouten, P. C. P.; Miedema, A. R. *Rep. Prog. Phys.* **1982**, *45*, 937−1039.
(45) Weaver, J.; Olson, C. *Phys. Rev. B* **1977**, *15*, 590−594.
(46) Weaver, J. *Phys. Rev. B* **1975**, *11*, 1416−1425.
(47) Bass, M.; DeCusatis, C.; Enoch, J.; Lakshminarayanan, V.; Li, G.; MacDonald, C.; Mahajan, V.; Van Stryland, E. *Handbook of Optics*, 3rd ed.; Vol. IV: Optical Properties of Materials, Nonlinear Optics, Quantum Optics (set); McGraw-hill: New York, 2009.
(48) Gartz, M.; Quinten, M. *Appl. Phys. B: Lasers Opt.* **2001**, *73*, 327−332.
(49) Liu, N.; Weiss, T.; Mesch, M.; Langguth, L.; Eigenthaler, U.; Hirscher, M.; Sönnichsen, C.; Giessen, H. *Nano Lett.* **2010**, *10*, 1103−1107.
(50) Tittl, A.; Mai, P.; Taubert, R.; Dregely, D.; Liu, N.; Giessen, H. *Nano Lett.* **2011**, *11*, 4366−4369.
(51) Griessen, R.; Giebels, I. A. M. E.; Dam, B. In *Hydrogen as a Future Energy Carrier*; Zttel, A., Borgschulte, A., Schlapbach, L., Eds.; Wiley-VCH Verlag GmbH & Co. KGaA: Weinheim, Germany, 2008; pp 275−334.
(52) Lee, M. W.; Shin, W. P. *J. Appl. Phys.* **1999**, *86*, 6798.
(53) Fu, Y. H.; Kuznetsov, A. I.; Miroshnichenko, A. E.; Yu, Y. F.; Luk'yanchuk, B. *Nat. Commun.* **2013**, *4*, 1527.
(54) Kuznetsov, A. I.; Miroshnichenko, A. E.; Fu, Y. H.; Zhang, J.; Luk'yanchuk, B. *Sci. Rep.* **2012**, *2*, 492.

(55) Azofeifa, D. E.; Clark, N.; Vargas, W. E.; Solís, H.; Pálsson, G. K.; Hjörvarsson, B. *J. Alloys Compd.* **2013**, *580*, 114.
(56) Messina, T.; Miller, C.; Markert, J. *Phys. Rev. B* **2007**, *75*, 104109.
(57) Richardson, T. J.; Slack, J. L.; Armitage, R. D.; Kostecki, R.; Farangis, B.; Rubin, M. D. *Appl. Phys. Lett.* **2001**, *78*, 3047.
(58) den Broeder, F. J. A.; van der Molen, S. J.; Kremers, M.; Huiberts, J. N.; Nagengast, D. G.; van Gogh, A. T. M.; Huisman, W. H.; Koeman, N. J.; Dam, B.; Rector, J. H.; Plota, S.; Haaksma, M.; Hanzen, R. M. N.; Jungblut, R. M.; Duine, P. A.; Griessen, R. *Nature* **1998**, *394*, 26−28.
(59) Griessen, R.; Huiberts, J. N.; Kremers, M.; van Gogh, A. T. M.; Koeman, N. J.; Dekker, J. P.; Notten, P. H. L. *J. Alloys Compd.* **1997**, *253*−*254*, 44−50.
(60) Lohstroh, W.; Westerwaal, R.; Noheda, B.; Enache, S.; Giebels, I. A. M. E.; Dam, B.; Griessen, R. *Phys. Rev. Lett.* **2004**, *93*, 197404.

dx.doi.org/10.1021/nl403643v | *Nano Lett.* 2014, 14, 1140−1147